INTERNATIONAL JOURNAL OF INTEGRATED ENGINEERING
ISSN: 2229-838X e-ISSN: 2600-7916

IJIE

Vol. 17 No. 1 (2025) 60-71
https://publisher.uthm.edu.my/ojs/index.php/ijie

CFD Investigation on the Influence of Roof Box Cargo Carrier Designs on Automobile Aerodynamics

Muhammad Amirul Hisamuddin[1], Izuan Amin Ishak[1]*, Mohammad Arafat[1], Razlin Abd Rashid[2], Ahmad Faiz Mohammad[3], Nor Afzanizam Samiran[4], Nor Atiqah Zolpakar[5]

[1] *Faculty of Engineering Technology, Universiti Tun Hussein Onn Malaysia, Education Hub Pagoh, 84600, Pagoh, MALAYSIA*
[2] *Department of Chemical Engineering, The University of Manchester, Manchester, M13 9PL, UNITED KINGDOM*
[3] *Department of Mechanical Precision Engineering, Malaysia-Japan International Institute of Technology (MJIIT), Universiti Teknologi Malaysia (UTM), Jalan Sultan Yahya Petra, 54100, Kuala Lumpur, MALAYSIA*
[4] *Faculty of Mechanical Engineering, Universiti Tun Hussein Onn Malaysia, Persiaran Tun Dr. Ismail, 86400 Parit Raja, Johor, MALAYSIA*
[5] *Faculty of Mechanical & Automotive Engineering Technology, Universiti Malaysia Pahang, 26600 Pekan, Pahang, MALAYSIA*

*Corresponding Author: izuan@uthm.edu.my
DOI: https://doi.org/10.30880/ijie.2025.17.01.005

Article Info

Received: 19 August 2024
Accepted: 11 April 2025
Available online: 30 April 2025

Keywords

Aerodynamic, airflow, roof box, fuel economy, computational fluid dynamic (CFD)

Abstract

In recent years, roof carrier boxes have become increasingly popular among travelers and larger families for their added luggage capacity. While these boxes address insufficient boot space, they also increase the vehicle's frontal area, adversely affecting aerodynamics and increasing drag. Given that aerodynamics significantly impacts vehicle efficiency, the design of the roof box is critical in determining drag force. This study aims to minimize drag to enhance fuel economy by utilizing ANSYS, a commercial Computational Fluid Dynamics (CFD) software, to analyze the coefficient of drag (C_d) for a numerical car model equipped with three different roof box designs in three locations, as well as in the absence of a roof box. The simulation employs Reynolds Averaged Navier-Stokes (RANS) equations in combining with the k-ε turbulence model. Concerning the stability of the vehicle influenced by the addition of the roof box, force coefficients, including drag and lift coefficients, were assessed. Results indicated that the drag and lift coefficients were highest at a speed of 25.5 m/s for all roof box configurations. The maximum C_d (0.4423) occurred with the XL model in the far backward position, while the highest C_l (0.4169) was observed with the Alpine model centrally positioned. Flow structure analysis highlighted vortex formation and wake turbulence at the vehicle's rear. Among the designs, the XL model in the central position was the most aerodynamically efficient, closely matching the base car's C_d and exhibiting the lowest C_l.

1. Introduction

Roof box cargo carriers are a popular type of additional vehicle storage used nowadays, especially for newer vehicles with limited trunk space [1]. Due to the lack of storage, most factories now have taken the initiative to reduce the problem by marketing the product of the roof box cargo carrier. Applying the roof box on the top of the vehicle will have some effect on the vehicle which affects the aerodynamics of the vehicle, especially the drag and lift of the vehicle because the roof of the vehicle is the sensitive parameter [2]. In a study by Dzijan et al., [3] they used CFD to analyze the aerodynamics of a closed-wheel race car. The realizable k-ε turbulence model and nonequilibrium wall functions were employed to compute a continuous viscous fluid flow. Their findings indicated that adjusting the front and rear ground clearances had a notable impact on aerodynamic drag and lift forces . The use of CFD revealed an increase in both drag and lift forces with variations in the surface's ground clearance [4]. Aerodynamics is the study of airflow and the motion of objects. It can be subdivided into external and internal aerodynamics [5], [6]. External aerodynamics pertains to the flow around the exterior compartment of a solid body, while internal aerodynamics focuses on the flow within an interior compartment. In a study by Kamal et al., [7] they used CFD to examine the flow structure of a simplified compact car in crosswind conditions. The results revealed that side force coefficients and rolling moments, which contribute to the risk of rollovers, are significant. The CFD predictions showed a small 3.3% error, and the side force coefficient increased as the sideslip angle (Ψ) reached 60°. This suggests that the findings align closely with previous transportation studies on lorries and vans regarding trends in aerodynamic loads and flow structures [7], [8].

Aerodynamic drag influences directional stability, fuel efficiency, and overall performance. If the drag force becomes higher it will cause fuel consumption of the vehicle and will make driving less safe [9], [10]. The position of of box is also important when using the roof box as the external storage for the vehicle because of the stability of the vehicle when driving at high velocity [11]. In a study by Schuetz et al. they found that adding racks increases the drag coefficient (C_d) by 9%. If a roof box is placed on the same rack, the C_d rises by 24%, and increases of up to 30% are not uncommon [12]. The addition of roof-mounted cargo boxes has been shown to markedly increase aerodynamic drag, with reported increases ranging from 40% to over 58% depending on the design and positioning of the cargo carrier [13]. This increase in drag directly correlates with a reduction in fuel efficiency; for instance, a study indicated that a sedan experienced a 25% decrease in fuel efficiency at highway speeds of 70 mph when equipped with a roof-mounted cargo box. Adding any object to the car roof is a highly influential factor, as evidenced by the 9% increase in C_d when racks are added. Studies have shown that the flow separation caused by roof-mounted cargo can exacerbate drag, particularly in vehicles with square-back designs, where the wake structure contributes significantly to overall aerodynamic drag [14]. Techniques such as vortex generators and tapered designs have been proposed to mitigate these effects, enhancing the overall aerodynamic profile of vehicles equipped with roof cargo carriers [15], [16].

Although roof box cargo carriers are widely used, previous studies have primarily focused on general aerodynamic effects without detailed analysis of different designs and locations on vehicles. This study fills this gap by providing a comprehensive CFD analysis of three distinct roof box designs positioned in various locations, offering new insights into how design and placement influence aerodynamic performance. In this study, computational fluid dynamics (CFD) combined with Reynold-Averaged Navier Stokes Equation (RANS) is applied as the numerical simulation.

2. Methodology

2.1 Research Framework

Figure 1 illustrates the overall process flowchart and CFD analysis. The 3D model for the vehicle is created as shown in Figure 2 and Figure 3 shows the 3D model for three types of roof boxes. The scale for the MPV model and the roof box is 1:1 scale as shown in Figure 2 and Figure 3 [17], [18], [19]. Following the completion of geometry modelling, a boundary and enclosure for simulation is generated in ANSYS. The validation process then begins with a grid independence test and mesh simulation based on the reference paper. The validation process is completed by running simulation with a different type of meshes which are from course meshes to finest meshes [20]. The analysis concentrated on the aerodynamic loads and flow structure around the roof box with the different locations and different locations of the roof box. The study investigates the aerodynamic performance of three distinct roof box designs-Sport Roof Box, XL Roof Box, and Alpine Roof Box; each with unique dimensions that impact their aerodynamic characteristics. The Sport Roof Box features a compact profile measuring 1.90 m in length, 0.629 m in width, and 0.425 m in height. In contrast, the XL Roof Box is slightly larger, with dimensions of 2.10 m in length, 0.587 m in width, and 0.613 m in height. The Alpine Roof Box, being the longest and narrowest, measures 2.254 m in length, 0.648 m in width, and 0.414 m in height. This study aims to explore how these varying shapes and sizes influence aerodynamic drag when the boxes are attached to vehicles, which is important for minimizing drag.

Int. Journal of Integrated Engineering Vol. 17 No. 1 (2025) 60-71

The simulations were conducted on a PC equipped with an Intel i7 processor featuring 8 cores and a total of 16 GB of RAM. Each of the three roof box designs—Sport, XL, and Alpine—was subjected to 1000 iterations to ensure robust and reliable aerodynamic performance results. The computational requirements for these simulations were significant, leading to a total processing time of approximately 4 hours for each case. Once the simulations were completed, the results were extracted and analyzed using ANSYS CFD Post software, which facilitated detailed visualization and interpretation of the aerodynamic characteristics, including drag coefficients and flow patterns around each roof box design.

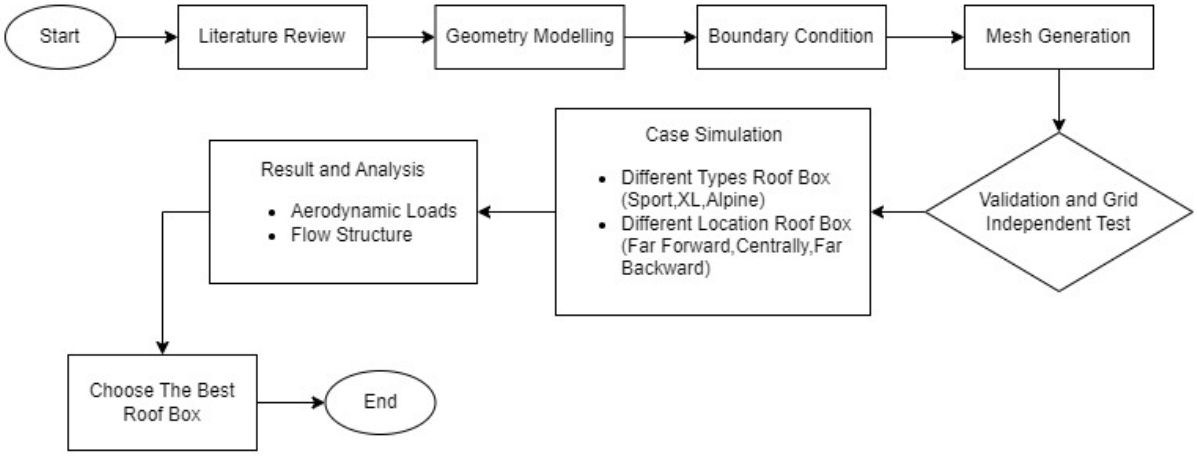

Fig. 1 *Flowchart of CFD analysis*

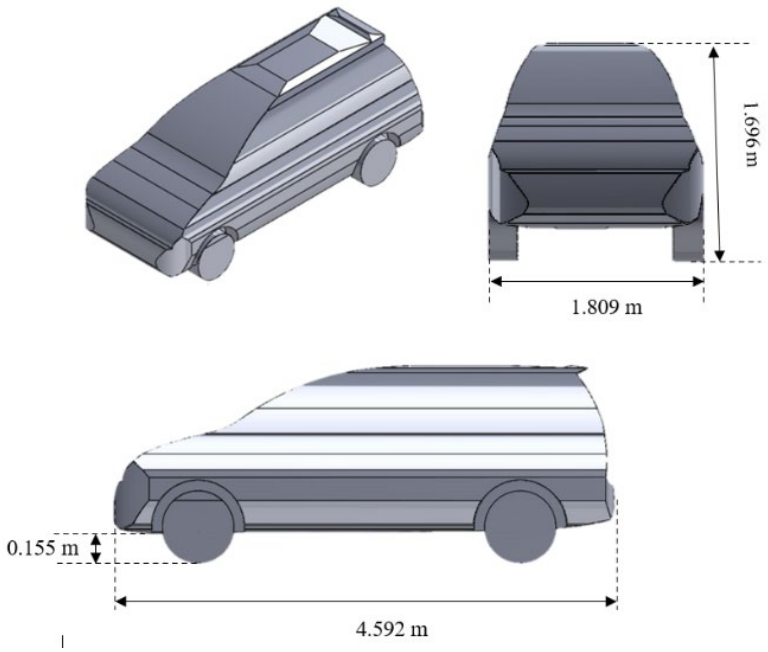

Fig. 2 *The dimensions of the MPV car*

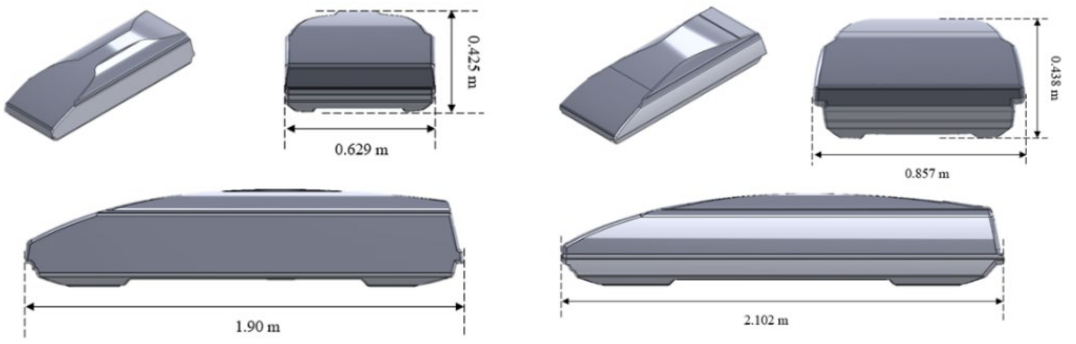

(a) **(b)**

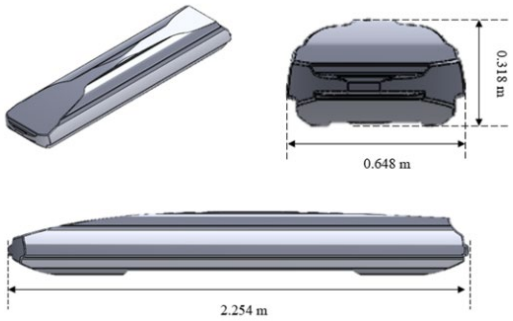

(c)

Fig. 3 *The dimensions of the roof box (a) Sport roof box; (b) XL roof box; (c) Alpine roof box*

2.2 Enclosure and Boundary Conditions

To provide a better mesh and more precise findings, a larger enclosure was constructed. The fluid domain or enclosure is used by analytical tools to mimic fluid. Figure 4 shows the vehicle model inside the enclosure.

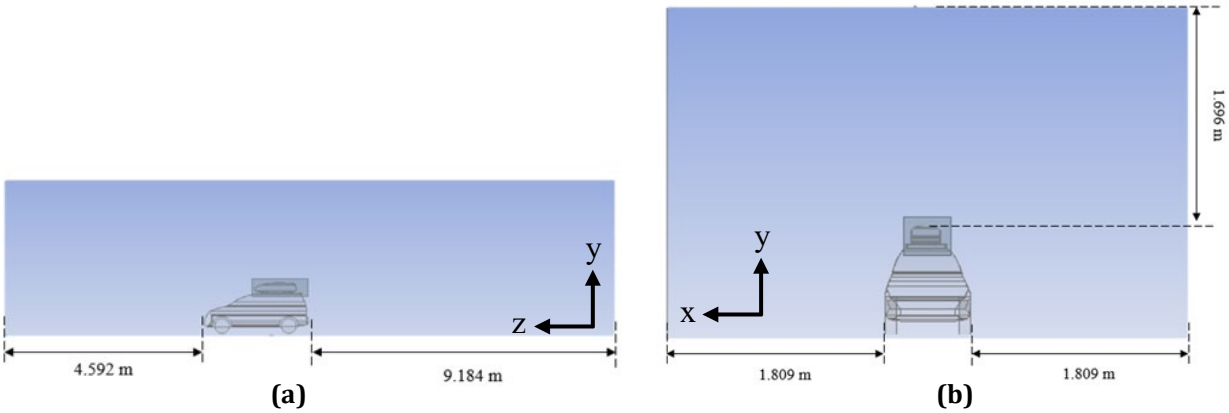

Fig. 4 *The enclosure (a) Side view; (b) Front view of the car with the roof box*

The boundary conditions used in the simulation were chosen to replicate real-world driving conditions. The velocity inlet was set to 25.5 m/s, representing highway driving speeds, and the pressure outlet was set to atmospheric pressure. These conditions allowed for a realistic representation of the aerodynamic forces acting on the roof box during typical vehicle operation. The model's boundary conditions, such as velocity inlet, pressure outlet, and vehicle surface, are established once the enclosure has been created as shown in Figure 5. The Reynolds number used in this investigation is Re = 2.7 x 10^6 which is calculated by inlet velocity and the characteristics length(car height) of the car and other details of boundary conditions are provided in Table 1 [21], [22]. The Realizable k-ε model was selected for this study due to its proven capability in capturing complex flow structures, especially in external aerodynamic flows, while maintaining reasonable computational cost. Comparative tests with Spalart-Allmaras and SST k-ω models showed negligible differences in the prediction of key aerodynamic parameters, justifying the selection of the Realizable k-ε model.

Int. Journal of Integrated Engineering Vol. 17 No. 1 (2025) 60-71

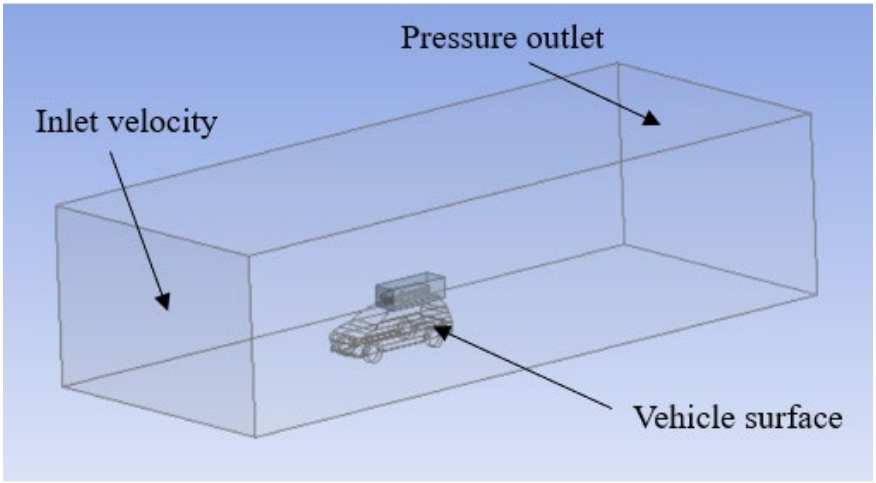

Fig. 5 *The numerical simulation boundary conditions*

Table 1 *Boundary conditions parameters*

Details	Boundary Condition	Value
Inlet	Inlet velocity	25.5 m/s
Outlet	Pressure outlet	0 Pa (gauge)
Wall	Wall boundary	Free slip wall
Vehicle Surface	Wall boundary	No sip wall

2.3 Grid Independence Study

The CFD results were validated through a mesh refinement study, where the coefficient of drag (C_d) was calculated using three distinct mesh types: coarse, medium, and fine. This process was not directly compared to experimental data but focused on achieving consistent numerical results as mesh refinement increased. The Cd values obtained were also compared with typical drag coefficients for standard vehicles, such as a mid-size MPV (which typically has a Cd range of 0.3 to 0.4), to ensure that the simulated values were within a reasonable range for similar aerodynamic conditions. Mesh parameters were changed to create coarse, medium and fine mesh types as shown in Table 2 and the changes in result for each type of mesh were recorded as shown in Table 2. The value of C_d started to converge after the medium mesh, where percentage difference between medium and fine mesh was 0.02874. Although further refinement to the fine mesh produced nearly identical results, with both the medium and fine meshes yielding a minimal percentage error of 0.02874, the computational cost and resource requirements increased without significant improvement in accuracy. Therefore, the medium mesh provided an optimal balance between accuracy and computational efficiency, making it the preferred choice for validation.

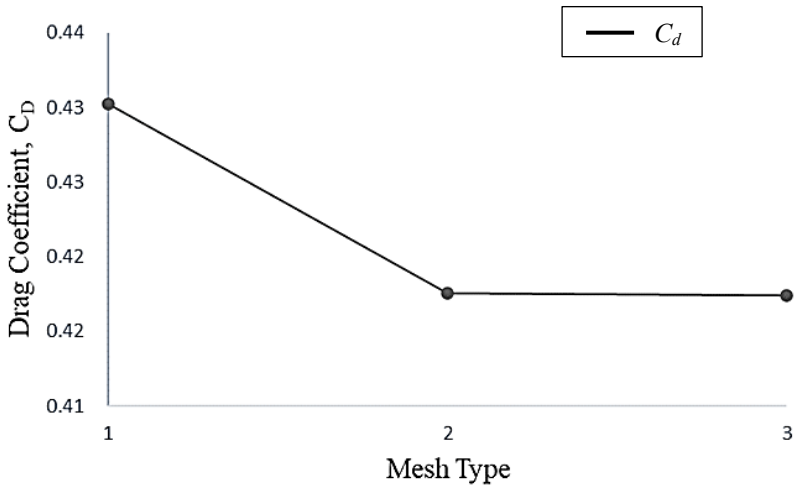

Fig. 6 *Graph of drag coefficient for 3 mesh resolution*

Table 2 *Parameters used for validation*

Mesh type	Course	Medium	Finest
	Mesh 1	Mesh 2	Mesh 3
Element size (mm)	1,200	600	300
Body sizing (mm)	500	400	300
Face sizing (mm)	1,600	800	400
Number of elements	360,861	872,707	1,908,111
Number of nodes	1,813,572	4,500,875	10,261,762
Drag coefficient (C_d)	0.43	0.42	0.42
Percentage error (%)	3.04	0.02874	

3. Results and Discussion

The results were analyzed in two main categories which the quantitative results including the coefficient of aerodynamic forces like drag coefficient and lift coefficient with the various types of roof boxes and location of the roof boxes and the qualitative results include streamlines and vortex formations due to the changes in pressure acting on the roof box at the various of the position of the plane.

3.1 Quantitative Result

Figure 7(a), Figure 7(b), illustrate variations in the drag coefficient (C_d) and lift coefficient with different roof box types and locations, maintaining a velocity of 25.5 m/s. The data for various roof box types and locations are compared against a base model without a roof box, ensuring distinctions between using and not using a roof box. Referring to Table 7(a), the drag coefficient value (C_d) without a roof box is 0.4333. In the first location, with the roof box positioned far forward, the C_d values for the Sport and XL models decrease by 5.57% and 5.54%, respectively, while the Alpine model increases by 1.21%. In the central location, the data indicates a decrease of 0.84% and 1.55% for the Sport and Alpine models, with a 0.13% increase for the XL model. Moving to the far backward location, the Sport and Alpine models show a decrease in C_d values by 1.31% and 3.74%, while the XL model sees an increase of 2.09%.

The initial position is situated far forward, where all three roof box designs exhibit a decrease in lift coefficient (C_l): 30.33% for the Sport, 34.35% for the XL, and 36% for the Alpine design. Moving to the central location, two designs show a decrease in value by 36.89% and 46.26% for the Sport and XL designs, while the other design exhibits an increased value of 18.51% for the Alpine design. Finally, at the far backward position, two designs demonstrate a decreased value of 23.29% and 41.69% for the Sport and XL models, while the Alpine model shows an increased value of 7.98%.

In conclusion, based on the data from Figure 7(a), certain roof box models and positions exhibit potential for use in MPV cars, as they yield the lowest C_d values, and the lift coefficient (C_l) tends to increase when the drag coefficient (C_d) decreases. For example, in Figure 7(a), the drag coefficient (C_d) for the Alpine model is greater than the C_d value for the base model. However, Figure 7(b) reveals that the lift coefficient (C_l) is lower than that of the base model.

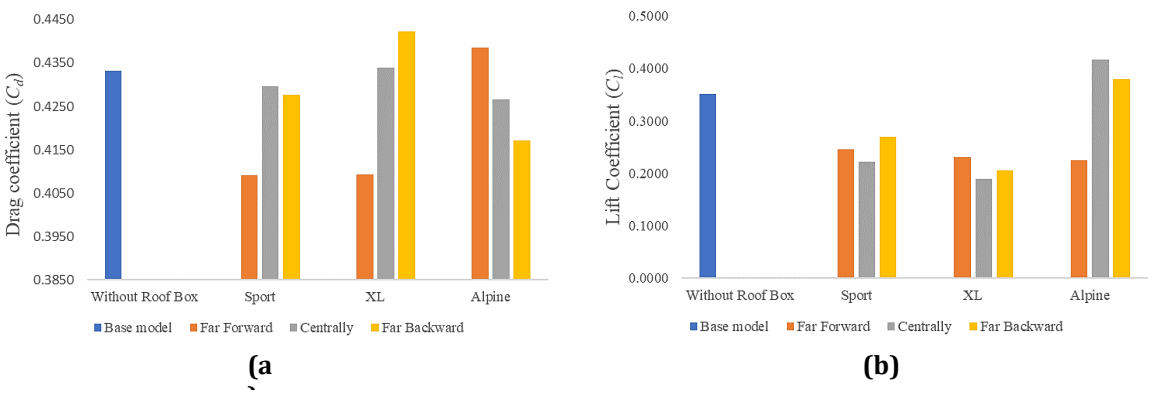

Fig. 7 *(a) Drag coefficient, C_d;(b) Lift coefficient, C_l for the different types of roof boxes and different locations of roof boxes*

Int. Journal of Integrated Engineering Vol. 17 No. 1 (2025) 60-71

3.2 Quantitative Result

This quantitative section will showcase the superimposition of streamlines onto pressure contours around both the car and the roof box. Streamlines depict the paths of individual fluid particles, while pressure contours represent regions of equal pressure. By combining these visual elements, we gain insights into the airflow around the car and the corresponding pressure distribution. The results will be presented for different axes, namely the x-axis, y-axis, and z-axis.

Figures 8(a-i), Figure 9(a-i), and Figure 10(a-i) display streamline pressure results, illustrating variations in streamlines. Figure 8(a-c), focused on the x-axis at 0m, reveals differences in turbulence for the Sports model, emphasizing increased wake turbulence vortex horizontally. This is evident in Figure 7(a), where the centrally located roof box generates more drag due to a smaller blue region at the rear compared to forward and backward positions. Vertically, the Sport and Alpine models create two vortices, while the XL model has a single vortex (Figure 8(d)). Moving horizontally with the XL model (Figure 8(d-f)), wake turbulence increases as the roof box is positioned farther back, influencing drag. However, the Alpine model, being more aerodynamic and longer, exhibits increased lift with the roof box moved backwards, as shown in Figure 7(a) for planes x = 0.2m and x = -0.26m, different vortex formations are observed at the car's rear.

As the roof box moves backwards, the turbulent boundary layer enlarges, especially for the Sport model (Figure 8(c)). In Figure 9 and Figure 10, the XL model at the central roof box location creates a larger reversed flow region and a reduced wake region (In Figure 9(e)) compared to forward and backward positions. In the Alpine model (Figure 9(g-i)), the flow separation at the back of the roof box becomes more unstable as it moves farther back, with a smaller vortex at the forward location than at centrally and backward locations. Figure 10(g-i) for the Alpine model indicates a decreasing vortex number as the roof box moves backwards. The figure clearly shows that mounting the cargo box Far Backward tends to result in smoother airflow and less intense pressure regions, which could translate into better fuel efficiency and reduced drag for all designs. The shape of the cargo box also matters. The Alpine Roof Box shows the most streamlined pressure distribution, likely leading to lower drag. On the other hand, the XL Roof Box, with its bulkier shape, generates the most significant high-pressure zones, leading to higher drag.

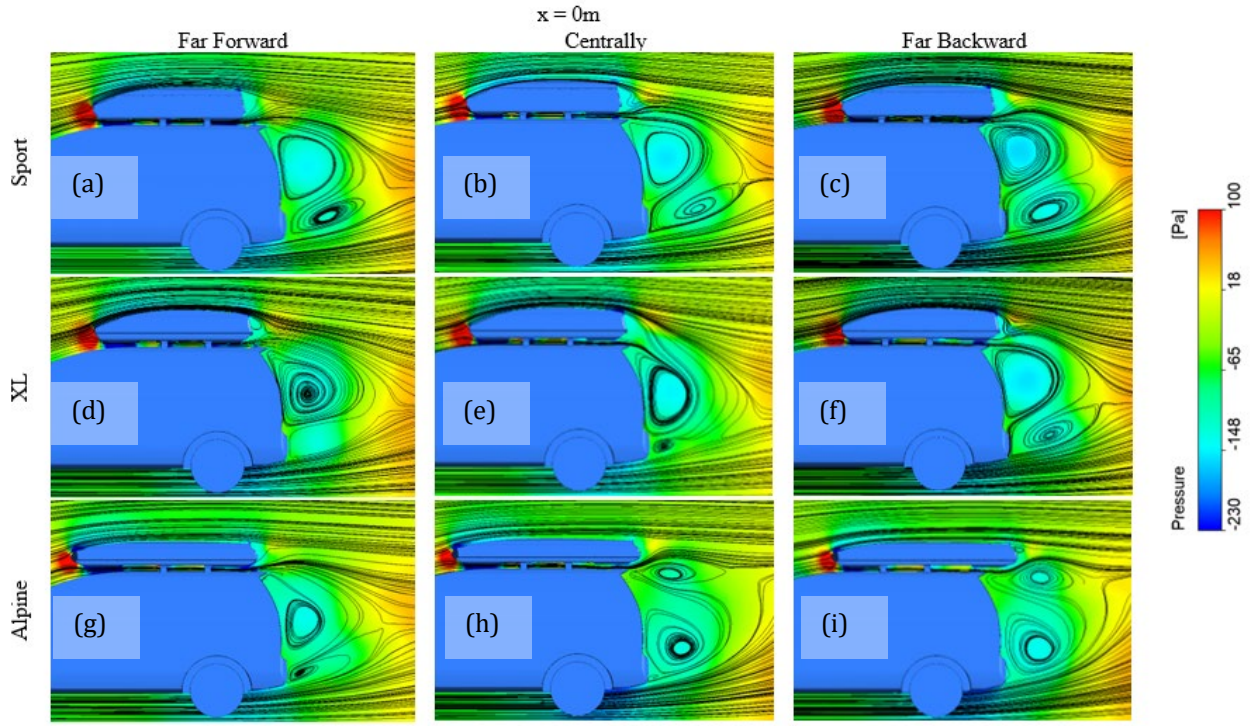

Fig. 8 *Streamlines superimposed on the pressure contour at the x = 0m*

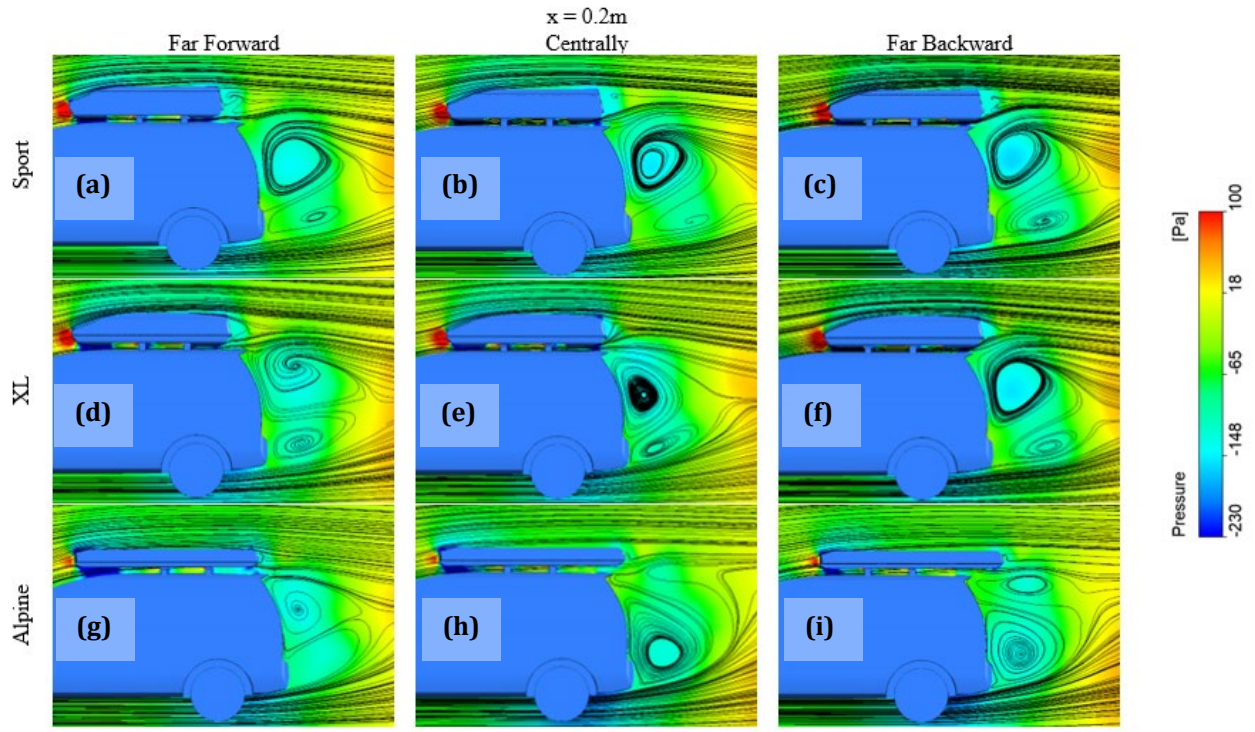

Fig. 9 *Streamlines superimposed on the pressure contour at the x = 0.2m*

Next, the first location to be discussed is at y = 1.1m, situated at the centre of the roof box. The findings reveal that streamlines are more widely spaced in the low-pressure area behind the object, indicating slower flow. Vertically, there's a decrease in the blue region on the left side of the bottom roof box for the Sport model, signifying increasing pressure as the roof box moves backwards. This pattern is consistent across other roof box models. Figure 11 illustrates vortex formation at the bottom rear of the car. For instance, in Figure 11 of the Sports model at the far forward location, no vortex is formed at the right bottom of the roof box, while Figure 4.6 shows a vortex at the bottom but not above the rear of the car.

The next discussion focuses on streamlines at the plane y = 0.95m. This location is chosen to observe the streamlined flow. The results show a larger blue area compared to the previous y = 1.1m location. Horizontally, the Sport model exhibits lower pressure on the right and left in the front area of the roof box compared to the Alpine and XL models. However, on the right side of the roof box, the Alpine model produces higher pressure than the Sport and XL models due to its smaller blue region. This pattern holds for central and far-back positions, where the Alpine model consistently generates higher pressure on the right side of the roof box compared to other models.

Int. Journal of Integrated Engineering Vol. 17 No. 1 (2025) 60-71

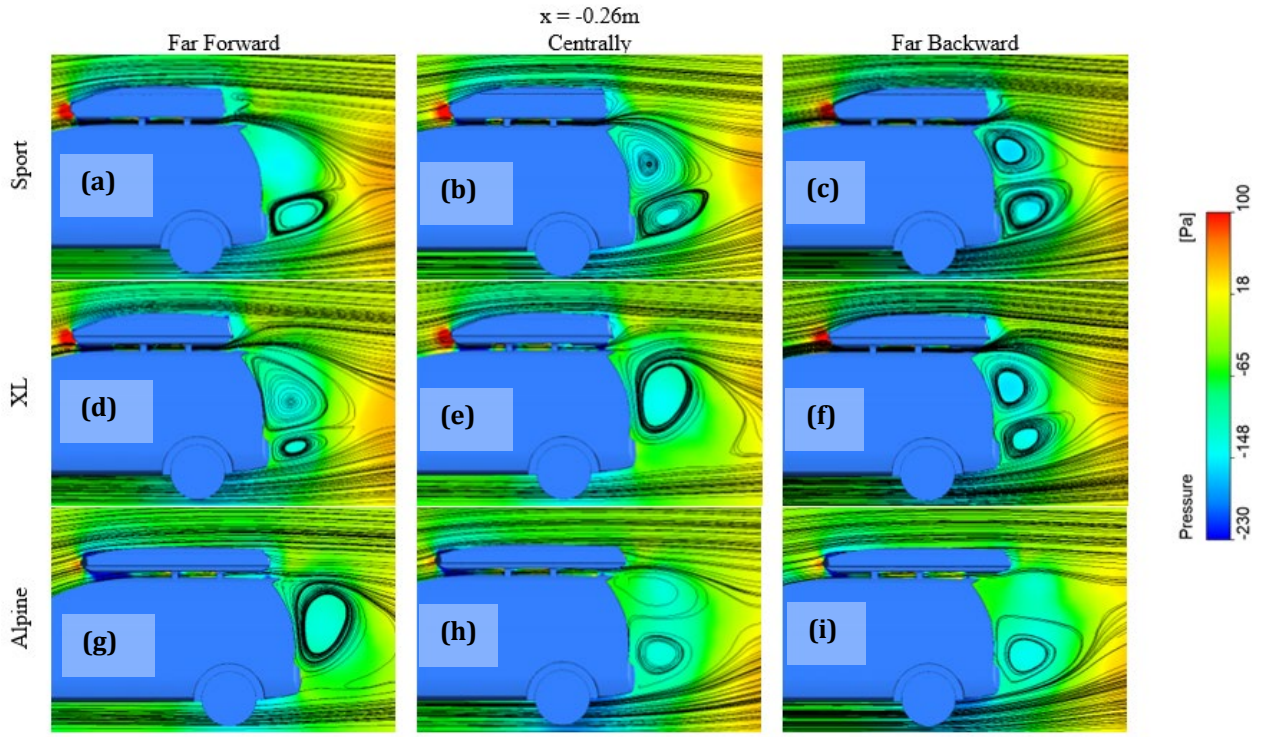

Fig. 10 *Streamlines superimposed on the pressure contour at the x = -0.26m*

The next location is on the z-axis, specifically at z = -1.65m. In Figure 12, there is an observed increase in pressure as the roof box is moved farther back. This is evident in the diminishing blue region on the left and right of the roof box for all three roof box models. For the Sport model, the boundary layer stagnation around the roof box expands as the roof box is positioned farther back. This is due to the streamlines flow, which initially goes through the bottom of the roof box at the far forward location but surrounds the surface of the roof box at centrally and far-back positions. The XL model exhibits a similar pattern, with the boundary layer stagnation increasing as the roof box is moved backwards.

Figure 12 depicts that at the far-back position, the vortex formation at the side of the roof box becomes more pronounced. The blue region at the bottom of the car indicates lower pressure, which leads to reduced downforce. Lower pressure beneath the car creates an upward force, potentially lifting the car slightly off the ground, thereby decreasing grip and handling, especially at high speeds [23]. This could also introduce instability, where very low pressure might lift the car off the ground, making it challenging to control. In the centrally located Sport model, Figure 12 reveals a smaller blue region, indicating higher pressure under the car compared to far forward and far backward positions. Finally, in the Alpine model, as the roof box is positioned farther back, the blue region under the car becomes brighter. Figure 7(b) illustrates that the lift increases as the roof box is moved further back.

Based on the data above, the varying roof box designs and positions impact the aerodynamic loads and the flow structure. Different designs and positions lead to distinct pressure patterns at the frontal area of the roof box, as illustrated in Figure 8, Figure 9, and Figure 10, indicating areas of high air velocity as the car passes through. Additionally, variations in aerodynamic loads are observed compared to the base model, with the XL model at the far backward position showing the highest C_d value and the Alpine model at the central position exhibiting the highest C_l value. Consequently, the XL model at the central location emerges as the optimal design, offering a C_d value closest to the base model and the lowest C_l value.

The numerical simulations conducted in this study provide critical insights into the aerodynamic behavior of roof boxes. These results can guide practical design improvements, such as modifying the shape of the roof box to minimize drag and improve fuel efficiency. Manufacturers could adopt these insights to create more aerodynamically efficient products for the automotive market.

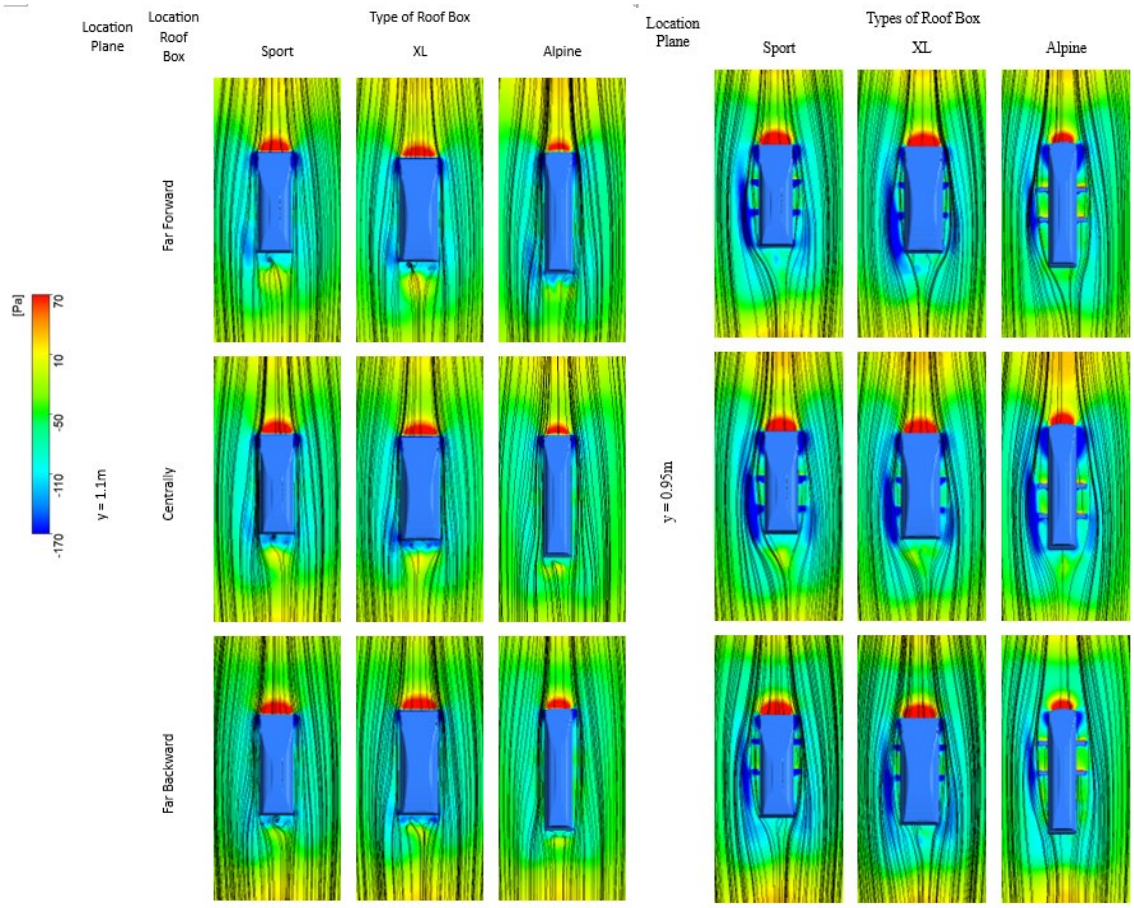

Fig. 11 *Streamlines superimposed on the pressure contour at the y = 1.1m (left) and y =0.95m (right)*

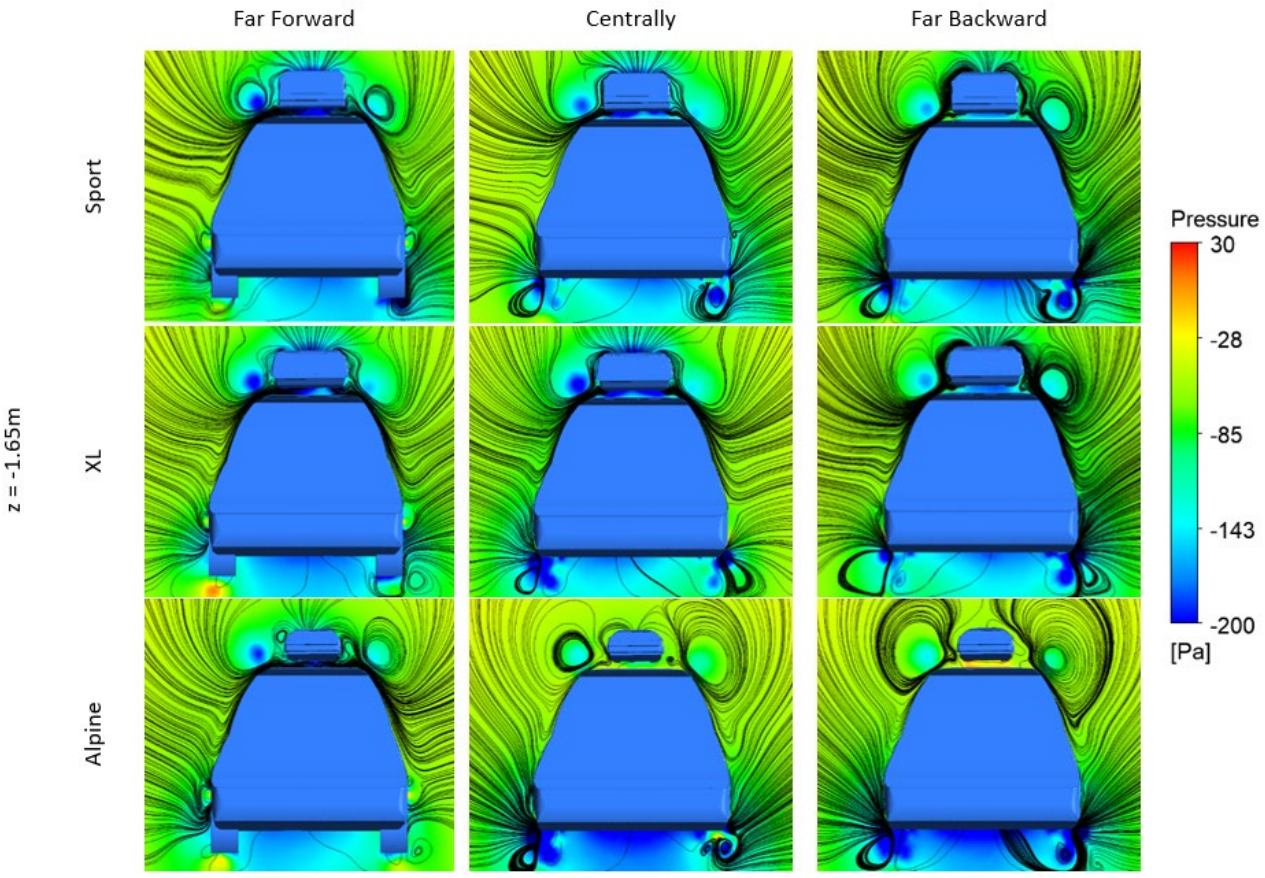

Fig. 12 *Streamlines superimposed on the pressure contour at the z = -1.65m*

4. Conclusion

This study investigated the aerodynamic effects of different roof box designs and positions on a vehicle using CFD simulations. Quantitative results showed that without a roof box, the drag coefficient (C_d) was 0.4333. Among the designs, the Sport and XL models reduced C_d by 5.57% and 5.54%, respectively, when placed in the far forward position, while the Alpine model increased it by 1.21%. In the far backward position, the Sport and Alpine models further reduced C_d by 1.31% and 3.74%, respectively, while the XL model increased it slightly. The lift coefficient (C_l) also decreased significantly, with the XL model centrally positioned showing the largest reduction of 46.26%. Visual analyses revealed how different positions affect the flow structure, with increased wake turbulence for the Sport model centrally placed and more stable flow for the Alpine model. Future work could explore real-world testing or simulations under varying driving conditions to further assess the aerodynamic impact of roof box designs.

Acknowledgement

This research was supported by Ministry of Higher Education (MOHE) through Fundamental Research Grant Scheme (FRGS/1/2024/TK10/UTHM/02/13).

Conflict of Interest

Authors declare that there is no conflict of interest regarding the publication of the paper.

Author Contribution

The authors confirm their contribution to the paper as follows: ***study conception and design:*** *Muhammad Amirul Hisamuddin, Izuan Amin Ishak;* ***data collection*** *Muhammad Amirul Hisamuddin, Mohammad Arafat;* ***analysis and interpretation of results*** *Muhammad Amirul Hisamuddin, Mohammad Arafat;* ***draft manuscript preparation:*** *Muhammad Amirul Hisamuddin, Izuan Amin Ishak, Nor Afzanizam Samiran, Razlin Abd Rashid, Ahmad Faiz Mohammad, Nor Atiqah Zolpakar. All authors reviewed the results and approved the final version of the manuscript.*

References

[1] M. F. Abdul Latif, M. N. Hashim, M. Z. . Rashid, M. A. Azhari, and M. N. Othman, "Roof Box Shape Streamline Adaptation and the Impact towards Fuel Consumption," *MATEC Web Conf.*, vol. 97, p. 01089, Feb. 2017, https://doi.org/10.1051/matecconf/20179701089.

[2] M. Sandberg, "Aerodynamic study of vehicle mounted cargo boxes," CHALMERS UNIVERSITY OF TECHNOLOGY, 2022. [Online]. Available: www.chalmers.se

[3] I. Džijan, A. Pašić, A. Buljac, and H. Kozmar, "Aerodynamic Forces Acting on a Race Car for Various Ground Clearances and Rake Angles," *J. Appl. Fluid Mech.*, vol. 12, no. 2, pp. 361–368, Mar. 2019, https://doi.org/10.29252/jafm.12.02.28706.

[4] S. Jamei, A. Maimun, S. Mansor, A. Priyanto, N. Azwadi, and M. Mobassher Tofa, "Aerodynamic Behavior of a Compound Wing Configuration in Ground Effect," *J. Teknol.*, vol. 66, no. 2, pp. 21–27, Jan. 2014, https://doi.org/10.11113/jt.v66.2478.

[5] A. Sadikin *et al.*, "A Comparative Study of Turbulence Models on Aerodynamics Characteristics of a NACA0012 Airfoil," *Int. J. Integr. Eng.*, vol. 10, no. 1, pp. 134–137, Apr. 2018, https://doi.org/10.30880/ijie.2018.10.01.019.

[6] S. Sarkar, K. Thummar, N. Shah, and V. Vagrecha, "A Review paper on Aerodynamic Drag Reduction and CFD Analysis of Vehicles," *Int. Res. J. Eng. Technol.*, vol. 6, no. 1, pp. 231–235, 2019, [Online]. Available: 10.13140/RG.2.2.31506.91849

[7] M. N. F. Kamal *et al.*, "Flow Structure Characteristics of the Simplified Compact Car Exposed to Crosswind Effects using CFD," *J. Adv. Res. Appl. Sci. Eng. Technol.*, vol. 28, no. 1, pp. 56–66, 2022, https://doi.org/10.37934/araset.28.1.5666.

[8] H. Eftekhari, A. S. M. Al-Obaidi, and S. Eftekhari, "The Effect of Spoiler Shape and Setting Angle on Racing Cars Aerodynamic Performance," *Indones. J. Sci. Technol.*, vol. 5, no. 1, pp. 11–20, Jan. 2020, https://doi.org/10.17509/ijost.v5i1.22701.

[9] J. Axelson *et al.*, "Aerodynamic Analysis and Improvement of a Roof Box Car," *Int. J. ...*, vol. 49, no. December, p. 13, 2014, [Online]. Available: http://www.ijens.org/Vol_14_I_02/145302-6868-IJMME-IJENS.pdf%5Cnhttp://www.sciencedirect.com/science/article/pii/B9780857095220500145%5Cnhttp://proceedings.asmedigitalcollection.asme.org/proceeding.aspx?doi=10.1115/FEDSM2012-72491%5Cnhttp://dx.doi.org/10.

[10] M. Andrés and A. Norkus, "Car-top cargo carrier aerodynamics," Universidad Pontificia Comillas, 2022.

[11] R. M. Janicki and A. Piechna, "Examining influence of a rooftop cargo carrier position on automobile aerodynamics," in *AIP Conference Proceedings*, 2019, p. 020073. https://doi.org/10.1063/1.5092076.
[12] T. Morel, "Aerodynamics of Road Vehicles.," *Fuel Econ Road Veh Powered by Spark Ignition Engines*, pp. 335–392, 1984, https://doi.org/10.1146/annurev.fluid.25.1.485.
[13] M. G. Connolly, M. J. O'Rourke, and A. Ivankovic, "A Drag Reduction Study on the Aerodynamics of the Irish Taxi Sign," *Fluids*, vol. 8, no. 9, p. 238, Aug. 2023, https://doi.org/10.3390/fluids8090238.
[14] A. K. Perry, M. Passmore, and A. Finney, "Influence of Short Rear End tapers on the Base Pressure of a Simplified Vehicle," *SAE Int. J. Passeng. Cars - Mech. Syst.*, vol. 8, no. 1, pp. 317–327, 2015, https://doi.org/10.4271/2015-01-1560.
[15] Y. Wang, C. Wu, G. Tan, and Y. Deng, "Reduction in the aerodynamic drag around a generic vehicle by using a non-smooth surface," *Proc. Inst. Mech. Eng. Part D J. Automob. Eng.*, vol. 231, no. 1, pp. 130–144, Jan. 2017, https://doi.org/10.1177/0954407016636970.
[16] M. Varney, M. Passmore, and A. Gaylard, "The Effect of Passive Base Ventilation on the Aerodynamic Drag of a Generic SUV Vehicle," *SAE Int. J. Passeng. Cars - Mech. Syst.*, vol. 10, no. 1, pp. 2017-01–1548, Mar. 2017, https://doi.org/10.4271/2017-01-1548.
[17] X. Shen, M. Lu, S. Fernando, and S. M. AbouRizk, "Tunnel boring machine positioning automation in tunnel construction," *Gerontechnology*, vol. 11, no. 2, Jun. 2012, https://doi.org/10.4017/gt.2012.11.02.558.00.
[18] A. H. Ariffin, Z. M. Jawi, Y. Ahmad, M. S. Solah, and F. Yusof, "Malaysian Vehicle Assessment Programme PROTON – A 4-Star MPV in Safety," 2009.
[19] T. E. Tezduyar, S. Sathe, and K. Stein, "Solution techniques for the fully discretized equations in computation of fluid–structure interactions with the space–time formulations," *Comput. Methods Appl. Mech. Eng.*, vol. 195, no. 41–43, pp. 5743–5753, Aug. 2006, https://doi.org/10.1016/j.cma.2005.08.023.
[20] M. Arafat, I. A. Ishak, and A. F. Mohammad, "Influence of mesh refinement on the accuracy of numerical results for Next-Generation High Speed Train," Muar, Unpublished, 2022. https://doi.org/10.31219/osf.io/85jdh.
[21] A. Al Saadi and A. Hassanpour, "Simulations of Aerodynamic Behaviour of a Super Utility Vehicle Using Computational Fluid Dynamics," *Adv. Automob. Eng.*, vol. 05, no. 01, 2016, https://doi.org/10.4172/2167-7670.1000134.
[22] R. M. Alves and O. de Almeida, "Validation of Experimental and Numerical Techniques for Flow Analysis over an Ahmed Body," *Int. J. Eng. Res. Appl.*, vol. 07, no. 04, pp. 63–71, Apr. 2017, https://doi.org/10.9790/9622-0704036371.
[23] S. Y. Cheng, M. Tsubokura, Y. Okada, T. Nouzawa, T. Nakashima, and D. H. Doh, "Aerodynamic stability of road vehicles in dynamic pitching motion," *J. Wind Eng. Ind. Aerodyn.*, vol. 122, pp. 146–156, Nov. 2013, https://doi.org/10.1016/j.jweia.2013.06.010.